Spectral Geometric Descriptor for Deformable 3D Shape Matching and Retrieval

Anis Kacem, Waleed Mohamed, and A. Ben Hamza

Concordia Institute for Information Systems Engineering
Concordia University, Montreal, QC, Canada

Abstract. We propose a spectral-geometric skeletal graph for nonrigid 3D shape retrieval. The skeleton is constructed from the isocontours of the second eigenfunction of the Laplace-Beltrami operator. We also introduce a graph matching mechanism based on a dissimilarity between the endpoints of the skeletal graph. Experimental results on a database of 3D models demonstrate the feasibility of our proposed framework.

Keywords: Deformable 3D shapes, retrieval, Laplace-Beltrami, shortest path.

1 Introduction

Recognition of 3D objects is becoming increasingly important due largely to the difficulty in processing information expeditiously without its recognition or identification. With the whopping increase in 3D scanners' usage and as a result of the latest developments in multimedia computing technologies, numerous databases of 3D models are distributed freely on the World Wide Web. The availability and widespread usage of such databases has sparked the need to efficiently search these 3D objects and retrieve the most relevant ones.

Recent years have witnessed a surge of interest in the spectral geometric analysis of the Laplace-Beltrami (LB) operator and its diverse applications to object recognition and shape analysis [1–3]. Reuter [1] proposed a shape registration and segmentation approach in the Morse-theoretic setting using the topological properties of the LB eigenfunctions. These eigenfunctions are determined via a cubic finite element method on mesh surfaces, and are arranged in increasing order of their associated eigenvalues. Rustamov [2] introduced the global point signature (GPS), which is defined as a vector whose elements are scaled eigenfunctions of the LB operator calculated at each surface point. GPS is isometric invariant, but it suffers from the problem of eigenfunctions switching whenever the associated eigenvalues are close to each other. Bronstein *et al.* [3] proposed a non-rigid shape retrieval approach using bags of features based on the heat kernel signature (HKS) [4]. HKS is a temporal shape descriptor for deformable shape analysis, and is defined as an exponentially-weighted combination of the LB squared eigenfunctions. HKS is a local shape descriptor that has a number of attractive properties, including robustness to small perturbations of the

M. Kamel and A. Campilho (Eds.): ICIAR 2013, LNCS 7950, pp. 181–188, 2013.

shape, efficiency, and invariance to isometric transformations. Shi *et al.* [5] used the level curves of the second eigenfunction of the LB operator to construct the spectral skeleton of 3D neuroanatomical structures. In addition to having a nice geometric property of following the pattern of the overall shape of a 3D object, the second eigenfunction of the LB operator captures well the intrinsic form of shapes, particularly the elongated ones (e.g. hippocampus) and it is also invariant to isometric transformations [5].

In this paper, we introduce a spectral geometric approach that aims at representing a 3D shape with a skeletal graph, which we refer to as the *Spectral Reeb Graph* (SRG). The core idea is to design a 3D shape descriptor from the Morse-theoretic perspective. To that end, the level sets (isocontours) of the second eigenfunction of the LB operator are first computed (identified); then each level set is encoded as a skeleton node representing the centroid of the isocontour.

The outline of this paper is as follows. In the next section, we introduce a spectral geometric framework for skeletal extraction from 3D shapes. Section 3 presents the skeleton-based graph matching algorithm based on the comparison of the relative shortest paths between the skeleton endpoints. The effectiveness of the spectral Reeb graph as a shape descriptor in nonrigid 3D shape retrieval is demonstrated in Section 4. In Section 5, we conclude with a summary.

2 Proposed Approach

Spectral geometry is concerned with the eigenvalue spectrum of the LB operator on a compact Riemannian manifold, and aims at describing the relationships between such a spectrum and the geometric structure of the manifold.

2.1 Laplace-Beltrami Operator

Let $\mathbb{M}$ denote a smooth orientable surface (2-manifold) embedded in the Euclidean space $\mathbb{R}^3$. A global parametric representation of $\mathbb{M}$ is a smooth vector-valued map $\boldsymbol{x}$ defined from a connected open set $U \subset \mathbb{R}^2$ to $\mathbb{M} \subset \mathbb{R}^3$ such that $\boldsymbol{x}(\boldsymbol{u}) = \big(x^1(\boldsymbol{u}), x^2(\boldsymbol{u}), x^3(\boldsymbol{u})\big)$, where $\boldsymbol{u} = (u^1, u^2) \in U$.

Given a twice-differentiable function $f : \mathbb{M} \to \mathbb{R}$, the Laplace-Beltrami (LB) operator is defined by

$$\Delta_{\mathbb{M}} f = -\frac{1}{\sqrt{\det g}} \sum_{i,j=1}^{2} \frac{\partial}{\partial u^j} \left(\sqrt{\det g}\, g^{ij} \frac{\partial f}{\partial u^i} \right), \tag{1}$$

where the matrix $g = (g_{ij})$ is the Riemannian metric tensor on $\mathbb{M}$, and g^{ij} denote the elements of the inverse of g. The metric tensor g is an intrinsic quantity in the sense that it relates to measurements inside the surface.

2.2 Discrete Laplace-Beltrami Operator

The use of triangle meshes for 3D object modeling/representation has become the *de facto* standard in the vast majority of computer graphics applications.

A triangle mesh $\mathbb{M}$ is usually denoted by $\mathbb{M} = (\mathcal{V}, \mathcal{T})$, where $\mathcal{V} = \{\boldsymbol{v}_1, \ldots, \boldsymbol{v}_m\}$ is the set of vertices and $\mathcal{T} = \{\boldsymbol{t}_1, \ldots, \boldsymbol{t}_n\}$ is the set of triangles. Two distinct vertices $\boldsymbol{v}_i, \boldsymbol{v}_j \in \mathcal{V}$ are adjacent (denoted by $\boldsymbol{v}_i \sim \boldsymbol{v}_j$ or simply $i \sim j$) if they are connected by an edge.

Using a mixed finite element/finite volume method on triangle meshes [6], the value of $\Delta_{\mathbb{M}} f$ at a vertex $\boldsymbol{v}_i$ can be approximated using the cotangent weight scheme:

$$\Delta_{\mathbb{M}} f(\boldsymbol{v}_i) \approx \frac{1}{a_i} \sum_{j \sim i} \frac{\cot \alpha_{ij} + \cot \beta_{ij}}{2} [f(\boldsymbol{v}_j) - f(\boldsymbol{v}_i)]$$

where α_{ij} and β_{ij} are the angles $\angle(\boldsymbol{v}_i \boldsymbol{v}_{k_1} \boldsymbol{v}_j)$ and $\angle(\boldsymbol{v}_i \boldsymbol{v}_{k_2} \boldsymbol{v}_j)$ of two faces $\boldsymbol{t}^\alpha = \{\boldsymbol{v}_i, \boldsymbol{v}_j, \boldsymbol{v}_{k_1}\}$ and $\boldsymbol{t}^\beta = \{\boldsymbol{v}_i, \boldsymbol{v}_j, \boldsymbol{v}_{k_2}\}$ that are adjacent to the edge $[i, j]$, and a_i is the area of the Voronoi cell (shaded polygon), as shown in Fig. 1. It should be noted that the cotangent weight scheme is numerically consistent and preserves several important properties of the continuous LB operator, including symmetry and positive-definiteness [7].

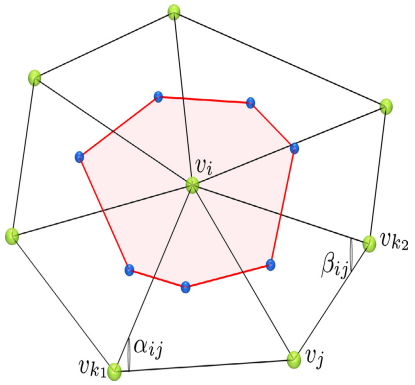

Fig. 1. Cotangent scheme

2.3 Spectral Skeleton

The eigenvalues λ_i and the associated eigenfunctions $\boldsymbol{\varphi}_i$ of the LB operator can be computed by solving the following generalized eigenvalue problem:

$$C\boldsymbol{\varphi}_i = \lambda_i R \boldsymbol{\varphi}_i, \quad i = 1, 2, \ldots, m \tag{2}$$

where $\boldsymbol{\varphi}_i$ is the unknown eigenfunction evaluated at m mesh vertices, $R = \mathrm{diag}(a_i)$ is a positive-definite diagonal matrix, and C is a sparse symmetric matrix given by

$$C = \begin{cases} \sum_{i=1}^{m} c_{ij} & \text{if } i = j \\ -c_{ij} & \text{if } i \sim j \\ 0 & \text{o.w.} \end{cases} \quad \text{with} \quad c_{ij} = \begin{cases} \dfrac{\cot \alpha_{ij} + \cot \beta_{ij}}{2} & \text{if } i \sim j \\ 0 & \text{o.w.} \end{cases} \tag{3}$$

We may sort the eigenvalues in ascending order as $0 = \lambda_1 < \lambda_2 \leq \cdots \leq \lambda_m$ with associated eigenfunctions as $\boldsymbol{\varphi}_1, \boldsymbol{\varphi}_2, \ldots, \boldsymbol{\varphi}_m$, where each eigenfunction $\boldsymbol{\varphi}_i$ is an m-dimensional vector.

Uhlenbeck [8] showed that the eigenfunctions of the LB operator are Morse functions on the interior of the domain of the operator. By a Morse function we mean a smooth function $f : \mathbb{M} \to \mathbb{R}$ such that all its singular (critical) points are nondegenerate. Morse theory explains the presence and the stability of the singular points of f in terms of the topology of $\mathbb{M}$.

An intriguing concept related to Morse theory is the so-called *Reeb graph*, which is defined as a quotient space $\mathbb{M}/\backsim$ with the equivalence relation given by $\boldsymbol{x} \backsim \boldsymbol{y}$ if and only if $f(\boldsymbol{x}) = f(\boldsymbol{y})$ and $\boldsymbol{x}, \boldsymbol{y}$ belong to the same connected

component of $f^{-1}(f(\boldsymbol{x}))$. An equivalence class is $[\boldsymbol{x}] = \{\boldsymbol{y} \in \mathbb{M} : \boldsymbol{x} \backsim \boldsymbol{y}\}$. Such classes are the connected components for the Reeb graph. Moreover, belonging to the same connected component is an equivalence relation given by

$$\boldsymbol{y} \backsim \boldsymbol{x} \Longleftrightarrow f(\boldsymbol{y}) = f(\boldsymbol{x}) \text{ and } \boldsymbol{x}, \boldsymbol{y} \in \mathcal{C}, \tag{4}$$

where $\mathcal{C}$ is the connected component of $f^{-1}(f(\boldsymbol{x}))$.

Consequently, the Morse function property of the eigenfunctions of the LB operator gives rise to constructing their associated Reeb graphs. As shown in Fig. 2(a), the second eigenfunction of the LB operator captures well the overall shape of the 3D horse model. Motivated by the isometry invariance property of the second eigenfunction of the LB operator and also by its generic property as a Morse function, we propose to use this eigenfunction to construct the spectral Reeb graph (shape skeleton) of a 3D object as follows: First, the level sets (isocontours) of the second eigenfunction are computed (identified), as depicted in Fig. 2(b); then each level set is encoded as a skeleton node representing the centroid of the isocurve, as shown in Fig. 2(c).

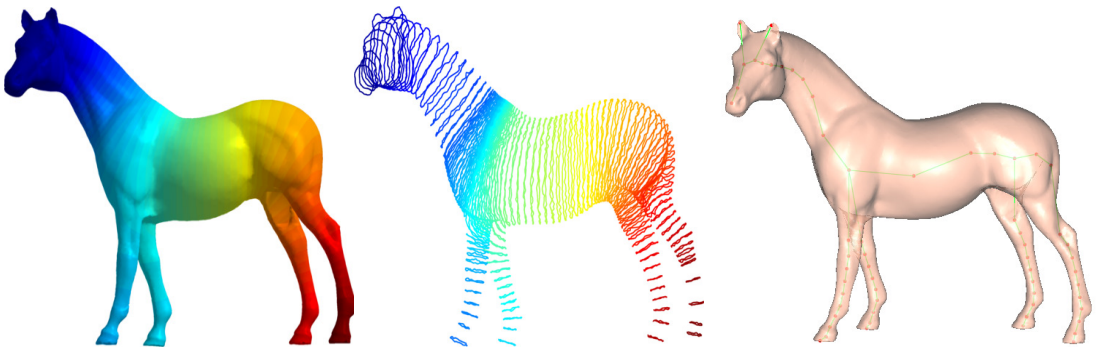

(a) (b) (c)

Fig. 2. (a) 3D horse model colored by $\boldsymbol{\varphi_2}$; (b) level sets of $\boldsymbol{\varphi_2}$; (c) spectral Reeb graph

3 Skeleton Endpoints Matching

In this section, we outline a skeleton graph matching mechanism via a dissimilarity measure that is defined by assigning geometric features to the endpoints of the skeletal graph [9]. This dissimilarity is defined in terms of the shortest paths between the endpoints of the spectral Reeb graphs. We refer to the skeleton node that is connected by only one edge as the *skeleton endpoint*, as illustrated in Fig. 3, where the endpoints are shown in blue color. It should be noted that endpoints are the salient points of the graph and may be viewed as visual parts of the 3D object. Thus, considering only the shortest paths between the skeleton endpoints would help dodge the instability issue with the skeleton junction points (i.e. points that have at least three neighboring points). To define our geometric dissimilarity measure, we use the shortest path between each endpoint and all other endpoints of the skeleton. The shortest path provides a valuable endpoint feature.

After constructing the 3D object skeleton, we then design a robust mechanism for graph matching. To that end, we perform graph matching by establishing a correspondence between endpoints of any two graphs [9]. Then, we perform pruning to eliminate non-salient nodes from the graph. Our matching approach consists of two main steps: (1) indexing, which reduces the number of skeletons to be compared with; and (2) we match the spectral Reeb graphs using a geometric dissimilarity to retrieve the closest shape.

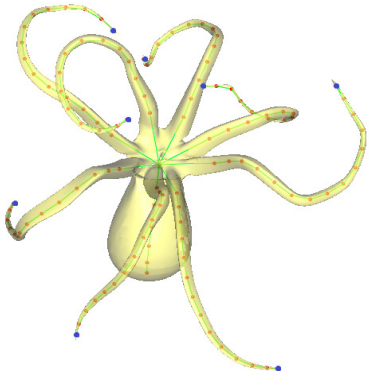

Fig. 3. Spectral Reeb graph of an octopus

Endpoint Features: After constructing the spectral Reeb graph of a 3D object, we then assign three distinct geometric features to each endpoint of the graph. The first geometric feature is the relative node area, which is defined as the area of the neighboring triangles of the endpoint divided by the total area of the 3D shape. The relative area feature provides valuable information about the endpoint. As a result, adding such a feature will help discriminate between endpoints based on the original 3D object and not just its skeleton. Additionally, the use of the relative area is largely credited to its invariance to scaling transformation. As a second feature, we assign the relative node path to to an endpoint. This feature is defined as the sum of shortest path distances from each endpoint to all other endpoints divided by the sum of the shorted paths from the mesh centroid (root node) to each endpoint. Finally, each endpoint is assigned a third feature called the relative centroid path, which corresponds to the shortest path from the mesh centroid to each endpoint, divided by the sum of the shortest paths from the mesh centroid to all the skeleton endpoints.

Endpoints Dissimilarity: Let G and $\widetilde{G}$ the spectral Reeb graphs of two 3D shapes $\mathbb{M}$ and $\widetilde{\mathbb{M}}$, respectively. The skeleton endpoints sets of G and $\widetilde{G}$ are denoted by $E = \{\boldsymbol{v}_i\}_{i=1,..,n_1}$ and $\widetilde{E} = \{\tilde{\boldsymbol{v}}_j\}_{j=1,..,n_2}$, respectively. We define the local dissimilarity measure between two endpoints $\boldsymbol{v}_i$ and $\tilde{\boldsymbol{v}}_j$ as the Euclidean distance

$$\Phi(\boldsymbol{v}_i, \tilde{\boldsymbol{v}}_j) = \|\boldsymbol{\omega}_i - \tilde{\boldsymbol{\omega}}_j\|, \tag{5}$$

between the 3D vectors $\boldsymbol{\omega}_i = (a_i, d\boldsymbol{v}_i, d\boldsymbol{c}_i)^T$ and $\tilde{\boldsymbol{\omega}}_j = (\tilde{\boldsymbol{v}}_j, d\tilde{\boldsymbol{v}}_j, d\tilde{\boldsymbol{c}}_j)^T$, whose components are defined by:

- a_i and $\tilde{a}_j$ are the relative node areas of $\boldsymbol{v}_i$ and $\tilde{\boldsymbol{v}}_j$
- $d\boldsymbol{v}_i = \sum_{k=1}^{n_1} \delta(\boldsymbol{v}_i, \boldsymbol{v}_k) / \sum_{k=1}^{n_1} \delta(\boldsymbol{c}, \boldsymbol{v}_k)$ and $d\tilde{\boldsymbol{v}}_j = \sum_{k=1}^{n_2} \delta(\tilde{\boldsymbol{v}}_j, \tilde{\boldsymbol{v}}_k) / \sum_{k=1}^{n_2} \delta(\tilde{\boldsymbol{c}}, \tilde{\boldsymbol{v}}_k)$ are the relative node paths of $\boldsymbol{v}_i$ and $\tilde{\boldsymbol{v}}_j$
- $d\boldsymbol{c}_i = \delta(\boldsymbol{c}, \boldsymbol{v}_i) / \sum_{k=1}^{n_1} \delta(\boldsymbol{c}, \boldsymbol{v}_k)$ and $d\tilde{\boldsymbol{c}}_j = \delta(\tilde{\boldsymbol{c}}, \tilde{\boldsymbol{v}}_j) / \sum_{k=1}^{n_2} \delta(\tilde{\boldsymbol{c}}, \tilde{\boldsymbol{v}}_k)$ are the relative centroid paths of $\boldsymbol{v}_i$ and $\tilde{\boldsymbol{v}}_j$
- $\boldsymbol{c}$ and $\tilde{\boldsymbol{c}}$ are the centroids of $\mathbb{M}$ and $\widetilde{\mathbb{M}}$, respectively
- $\delta(\cdot, \cdot)$ is the Dijkstra's shortest path distance.

Therefore, the geometric dissimilarity between two spectral Reeb graphs is given by the distance:

$$\mathcal{D}(G,\widetilde{G}) = \sum_{i=1}^{n_1}\sum_{j=1}^{n_2} \Phi(\boldsymbol{v}_i, \tilde{\boldsymbol{v}}_j) = \sum_{i=1}^{n_1}\sum_{j=1}^{n_2} \|\boldsymbol{\omega}_i - \tilde{\boldsymbol{\omega}}_j\|. \tag{6}$$

Algorithm 1 shows in detail the main steps of the proposed framework.

Algorithm 1 Proposed graph matching approach

Given two 3D objects $\mathbb{M}$ and $\widetilde{\mathbb{M}}$

1: Construct the spectral Reeb graphs G and $\widetilde{G}$ of $\mathbb{M}$ and $\widetilde{\mathbb{M}}$, respectively
2: Perform pruning to clean-off non-salient nodes
3: Determine the skeleton endpoints sets $E = \{\boldsymbol{v}_i\}_{i=1,..,n_1}$ and $\widetilde{E} = \{\tilde{\boldsymbol{v}}_j\}_{j=1,..,n_2}$ of G and $\widetilde{G}$, respectively
4: **for** all endpoints $\{\boldsymbol{v}_i\}$ and $\{\tilde{\boldsymbol{v}}_j\}$ **do**
5: Compute the relative node areas a_i and $\tilde{a}_j$ of $\boldsymbol{v}_i$ and $\tilde{\boldsymbol{v}}_j$, respectively
6: Compute the relative node paths $d\boldsymbol{v}_i$ and $d\tilde{\boldsymbol{v}}_j$
7: Compute the relative centroid paths $d\boldsymbol{c}_i$ and $d\tilde{\boldsymbol{c}}_j$
8: **end for**
9: Determine the correspondence between the spectral Reeb graphs
10: Compute the geometric dissimilarity $\mathcal{D}(G,\widetilde{G})$.

4 Experimental Results

To assess the performance of our approach, we tested it on McGill's database [10]. This benchmark provides a 3D shape repository, which consists of 255 objects that are divided into ten categories. Sample shapes are displayed in Fig. 4.

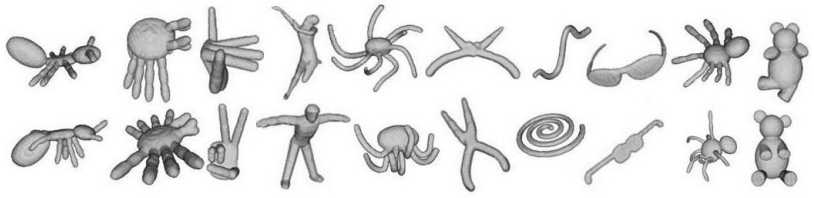

Fig. 4. Sample shapes from McGill Articulated Shape Database. Only two shapes for each of the 10 classes are shown.

The matching results on McGill's database are displayed in Table 1, which shows that our approach provides correct output results. A smaller value (displayed in boldface with a colored box around it for emphasis) of the geometric dissimilarity imply that the shapes are more similar.

Table 1. Matching results using our approach. Each database object is matched against all the other objects in the database. Each cell displays the geometric dissimilarity $\mathcal{D}(G, \widetilde{G})$ between two shapes selected from the benchmark. The smallest value corresponds to the correct match.

	0.0124	0.1127	0.1216	0.1258	0.1131	0.1344	0.1257
	0.1116	**0.0073**	0.1136	0.1297	0.1227	0.1124	0.1131
	0.1311	0.1142	**0.0653**	0.1356	0.1315	0.1171	0.1137
	0.1146	0.1329	0.1113	**0.0055**	0.1332	0.1621	0.1552
	0.1193	0.1248	0.1342	0.1421	**0.1131**	0.1572	0.1592
	0.1327	0.1109	0.1152	0.1474	0.11719	**0.1021**	0.1116
	0.1223	0.1128	0.1175	0.1453	0.1623	0.1121	**0.0042**

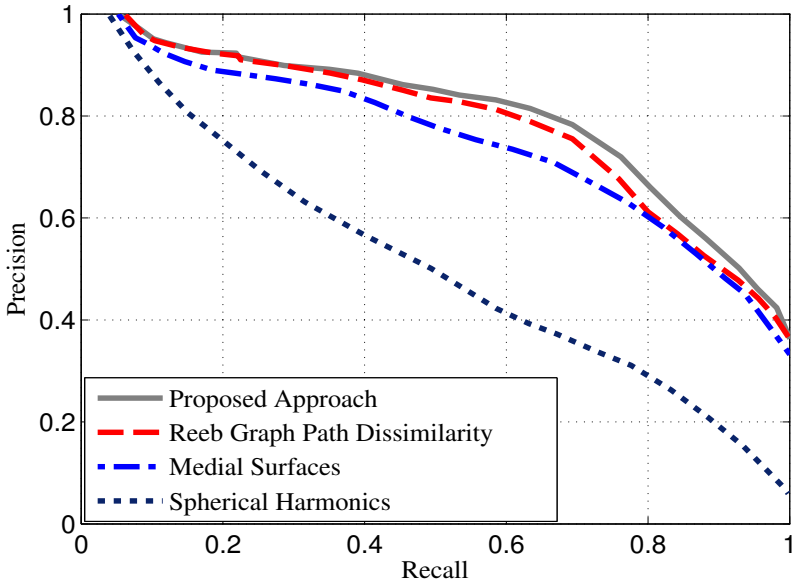

Fig. 5. Precision-Recall curves for spherical harmonics, medial surfaces, Reeb graph patch dissimilarity, and our approach on McGill's database

Additionally, we carried out a performance comparative study between our approach and existing methods, including spherical harmonics (SH) [11], medial surfaces (MS) [10], and Reeb graph patch dissimilarity (RGPD) method [9]. To that end, we performed experimental comparison on the entire benchmark by evaluating the performance of our approach via Precision *versus* Recall curve, which is a standard information retrieval evaluation measure. It should be noted that a Precision-Recall curve that is shifted upwards and to the right reveals superior retrieval performance. Our proposed framework outperforms spherical harmonics and medial surfaces, and performs slightly better than RGPD, as evinced by Fig. 5.

5 Conclusions

In this paper, we introduced a spectral geometric approach for 3D object matching and retrieval using a skeleton constructed from the second eigenfunction of the LB operator. The better performance of proposed framework was successfully demonstrated on McGill's articulated shape database in comparison with spherical harmonics, medial surfaces, and Reeb graph path dissimilarity method.

References

1. Reuter, M.: Hierarchical shape segmentation and registration via topological features of Laplace-Beltrami eigenfunctions. Int. Jour. Computer Vision 89(2), 287–308 (2010)
2. Rustamov, R.M.: Laplace-Beltrami eigenfunctions for deformation invariant shape representation. In: Proc. Symp. Geometry processing (SGP), pp. 225–233 (2007)
3. Bronstein, A.M., Bronstein, M.M., Guibas, L., Ovsjanikov, M.: Shape Google: Geometric words and expressions for invariant shape retrieval. ACM Trans. on Graphics 30(1) (2011)
4. Sun, J., Ovsjanikov, M., Guibas, L.: A concise and provably informative multi-scale signature-based on heat diffusion. Computer Graphics Forum 28(5), 1383–1392 (2009)
5. Shi, Y., Lai, R., Krishna, S., Sicotte, N., Dinov, I., Toga, A.W.: Anisotropic Laplace-Beltrami eigenmaps: Bridging Reeb graphs and skeletons. In: Proc. CVPR Workshops, pp. 23–28 (2008)
6. Meyer, M., Desbrun, M., Schröder, P., Barr, A.: Discrete differential-geometry operators for triangulated 2-manifolds. In: Visual Mathematics III, pp. 35–57 (2003)
7. Wardetzky, M., Mathur, S., Kälberer, F., Grinspun, E.: Discrete Laplace operators: no free lunch. In: Proc. SGP, pp. 33–37 (2008)
8. Uhlenbeck, K.: Generic properties of eigenfunctions. American Journal of Mathematics 98(4), 1059–1078 (1976)
9. Mohamed, W., Ben Hamza, A.: Reeb graph path dissimilarity for 3D object matching and retrieval. The Visual Computer 28(3), 305–318 (2012)
10. Siddiqi, K., Zhang, J., Macrini, D., Shokoufandeh, A., Bouix, S., Dickinson, S.: Retrieving articulated 3-D models using medial surfaces. Machine Vision and Applications 19(4), 261–275 (2008)
11. Kazhdan, M., Funkhouser, T., Rusinkiewicz, S.: Rotation invariant spherical harmonic representation of 3D shape descriptors. In: Proc. SGP, pp. 156–164 (2003)